

On the dynamical mechanism of cross-over from chaotic to turbulent states

G ANANTHAKRISHNA

Materials Research Centre and Centre for Condensed Matter Theory,
Indian Institute of Science, Bangalore 560 012, India
E-mail: garani@mrc.iisc.ernet.in

Abstract. The Portevin–Le Chatelier effect is one of the few examples of organization of defects. Here the spatio-temporal dynamics emerges from the cooperative behavior of the constituent defects, namely dislocations and point defects. Recent dynamical approach to the study of experimental time series reports an intriguing cross-over phenomenon from a low dimensional chaotic to an infinite dimensional scale invariant power-law regime of stress drops in experiments on CuAl single crystals and AlMg polycrystals, as a function of strain rate. We show that an extension of a dynamical model due to Ananthakrishna and coworkers for the Portevin–Le Chatelier effect reproduces this cross-over. At low and medium strain rates, the model shows chaos with the structure of the attractor resembling the reconstructed experimental attractor. At high strain rates, the model exhibits a power-law statistics for the magnitudes and durations of the stress drops as in experiments. Concomitantly, the largest Lyapunov exponent is zero. In this regime, there is a finite density of null exponents which itself follows a power law. This feature is similar to the Lyapunov spectrum of a shell model for turbulence. The marginal nature of this state is visualized through slow manifold approach.

Keywords. Chaos; power law; Lyapunov spectrum; Portevin–Le Chatelier effect; slow manifold.

PACS Nos 05.65.+b; 05.45.Ac; 62.20.Fe; 05.90.+m

1. Introduction

When spatially extended systems are driven away from equilibrium, they are known to give rise to spatio-temporal structures described usually by a few collective degrees of freedom. Consequently, there is a reduction in the effective dimension of the system. Despite this reduction, the system can exhibit complex dynamics such as chaos [1]. Dimensional reduction may not always be possible. In such situations, sometimes a scale-free correlated state with a power-law distribution of avalanches is seen. Most known power laws arise in slowly driven dissipative systems evolving naturally to a critical state without any tuning going by the name self-organized criticality (SOC) [2,3]. However, power laws are occasionally seen at high drives (as in hydrodynamics). In contrast to the infinite dimensional nature of the latter, chaos is low dimensional characterized by the self similarity of the strange attractor

and sensitivity to initial conditions. Thus, these two states are dynamically distinct [1–3] and hence they are rarely observed in the same system. Recently, a cross-over from chaos to power-law regime have been reported as a function of strain rate in experiments on the Portevin–Le Chatelier (PLC) effect [4,5]. The purpose of this report is to summarize our efforts to understand this cross-over dynamics within the framework of a model introduced by Ananthakrishna and coworkers [6].

The PLC effect or the jerky flow refers to a type of plastic instability seen when metallic alloys are deformed under constant strain rate $\dot{\epsilon}$ [7]. Here, one observes a series of yield drops accompanied by inhomogeneous deformation of the specimen. The effect is observed only in a window of strain rates and temperatures. The physical origin of the PLC effect is the competing time-scales corresponding to the dislocation mobility and that of the solute atoms, called dynamic strain aging (DSA) [7,8]. At low strain rates (or high temperatures) the average velocity of dislocations is low, and there is sufficient time for solute atoms to diffuse to the dislocations and pin them (aging). At high strain rates (or low temperatures), the time available for solute atoms to diffuse to the dislocations decreases and hence the stress required to unpin them decreases. However, in a range of strain rates and temperatures where these two time-scales are typically of the same order of magnitude, the PLC instability manifests. The competition between the slow rate of pinning and sudden unpinning of the dislocations, at the macroscopic level translates into a negative strain rate sensitivity (SRS) of the flow stress which is the basic instability mechanism used in most phenomenological models [7,9]. Each of the stress drops is generally associated with the nucleation and often propagation of a band of localized plastic deformation [7]. In polycrystals, these bands and the associated serrations are classified into three generic types C, B and A found with increasing strain rate or decreasing temperature.

The inherent nonlinearity and the presence of multiple time-scales demands the use of tools and concepts of nonlinear dynamical systems. While there is considerable theoretical work to understand this complex collective phenomenon [7], the first dynamical approach was taken in mid 80s by Ananthakrishna and coworkers [6]. Apart from predicting the generic features of the PLC effect, the model also predicted chaotic stress drops in a certain range of temperatures and strain rates [10] subsequently verified through a dynamical analysis of several data sets of experimental stress–time series [4,5,11,12]. Further experiments and analysis have showed an intriguing cross-over from chaotic to power-law state of stress drops in both single and polycrystals [4,5]. In addition, this cross-over is unusual in the sense that the only other example is the hydrodynamic turbulence [13]. In this paper, we present an extension of the Ananthakrishna’s model [6] to explain this cross-over in the PLC effect. Here, we concentrate on characterizing the dynamical causes responsible for this cross-over [14,15].

2. The Ananthakrishna’s model

The fully dynamical nature of the Ananthakrishna’s model makes it the most suitable model for studying this cross-over. (We emphasize here that there are no models that predict all the features of the PLC effect as well as chaotic stress drops

found in stress–time analysis.) Following the notation in [16], we present the evolution equations in terms of the scaled dislocation densities for the mobile $\rho_m(x, t)$, the immobile $\rho_{im}(x, t)$, and the Cottrell’s type $\rho_c(x, t)$. These equations are coupled to the rate of change of the scaled stress $\phi(t)$ using the machine equation. The equations are:

$$\frac{\partial \rho_m}{\partial t} = -b_0 \rho_m^2 - \rho_m \rho_{im} + \rho_{im} - a \rho_m + \phi_{\text{eff}}^m \rho_m + \frac{D}{\rho_{im}} \frac{\partial^2 (\phi_{\text{eff}}^m(x) \rho_m)}{\partial x^2}, \quad (1)$$

$$\frac{\partial \rho_{im}}{\partial t} = b_0 (b_0 \rho_m^2 - \rho_m \rho_{im} - \rho_{im} + a \rho_c), \quad (2)$$

$$\frac{\partial \rho_c}{\partial t} = c (\rho_m - \rho_c), \quad (3)$$

$$\frac{d\phi(t)}{dt} = d \left[\dot{\epsilon} - \frac{1}{l} \int_0^l \rho_m(x, t) \phi_{\text{eff}}^m(x, t) dx \right]. \quad (4)$$

The first term in eq. (1) refers to the annihilation or immobilization of two mobile dislocations, the second term to the annihilation of a mobile dislocation with an immobile one, and the third term to the re-mobilization of immobile dislocation due to stress or thermal activation. The fourth term represents the immobilization of mobile dislocations due to solute atoms. Once a mobile dislocation starts acquiring solute atoms we regard it as the Cottrell’s type dislocation ρ_c . As they progressively acquire more solute atoms, they eventually stop, and then they are considered as immobile dislocations ρ_{im} . The fifth term represents the rate of multiplication of dislocations due to cross-slip. This depends on the velocity of mobile dislocations which is taken to be $V_m(\phi) = \phi_{\text{eff}}^m$, where $\phi_{\text{eff}} = (\phi - h \rho_{im}^{1/2})$ is the scaled effective stress, m the velocity exponent and h a work hardening parameter. The non-local nature of the cross-slip gives rise to the last term, i.e., the spatial coupling term. (See for details, [14].) Here it suffices to note that the spatial term contains the factor ρ_{im}^{-1} and hence this term mimics the fact that cross-slip spreads only into regions of minimum back stress. Finally, a , b_0 and c are the scaled rate constants referring, respectively, to the concentration of solute atoms slowing down the mobile dislocations, the thermal and athermal reactivation of immobile dislocations, and the rate at which solute atoms are gathering around the mobile dislocations. In eq. (4), $\dot{\epsilon}$ is the scaled applied strain rate, d the scaled effective modulus of the machine and the sample, and l the dimensionless length of the sample.

The PLC state is reached through a Hopf bifurcation as in the original model. The domain of instability in $\dot{\epsilon}$ is $10 < \dot{\epsilon} < 2000$ for the parameter values $a = 0.8$, $b_0 = 0.0005$, $c = 0.08$, $d = 0.00006$, $m = 3.0$, $h = 0.07$ and $D = 0.5$ as shown in figure 1. Beyond this regime, uniform steady states exist. The numerical solutions of these equations are obtained by discretizing the specimen length into N equal parts and solving $3N + 1$ equations for $\rho_m(j, t)$, $\rho_{im}(j, t)$, $\rho_c(j, t)$, $j = 1, \dots, N$, and $\phi(t)$. The system size has been varied from $N = 100$ to 3333 with a view to investigate the convergence of the properties with the system size. The results discussed below hold true for a wide range of other parameters in instability domain including a range of values of D .

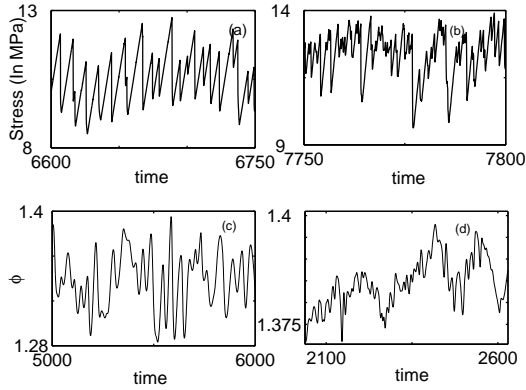


Figure 1. (a) and (b) Experimental stress–time series: (a) chaotic state at $\dot{\epsilon}_a = 1.7 \times 10^{-5} \text{ s}^{-1}$ and (b) SOC state at $\dot{\epsilon}_a = 8.3 \times 10^{-5} \text{ s}^{-1}$. (c) and (d) Stress–time series from the model at (c) $\dot{\epsilon} = 120$, (d) $\dot{\epsilon} = 280$.

3. Dynamical analysis

To begin with, consider the plots of two experimental stress–strain curves corresponding to the chaotic and power-law regimes of applied strain rates and time series from the model at intermediate and high strain rates (shown in figure 1). The visual similarity of the experimental time series at medium and high strain rates with that of the model in similar range of $\dot{\epsilon}$ is evident. The similarity extends to other dynamical features such as the nature of attractor as well. It was shown earlier in [4] that the stress–strain curve in figure 1a is chaotic with a correlation dimension, $\nu = 2.3$. Thus, the number of degrees of freedom required for the description of the dynamics of the system [17] is four in this case, consistent with the original model. Figure 2a shows a plot of the strange attractor obtained using singular value decomposition [18] of the experimental time series at applied strain rate $\dot{\epsilon}_a = 1.7 \times 10^{-5} \text{ s}^{-1}$. Here an appropriate combination of the first three principal directions of the subspace $C_i; i = 1-3$, has been used to facilitate comparison with the model. This can be compared with the strange attractor obtained from the model in the space of ρ_m, ρ_{im} and ρ_c ($j = 50$ and $N = 100$) shown in figure 2b for $\dot{\epsilon} = 120$ corresponding to the mid-chaotic region. Note the similarity with the experimental attractor, particularly the linear portion in the phase space (shown by an arrow in figure 2a) which can be identified with the loading direction in figure 1a. Note that the identification of the loading direction is consistent with the absence of growth of ρ_m .

As stated earlier, the time series at high strain rates shown in figure 1b exhibits a power law for distribution of stress drop magnitudes [4,5]. The stress–time series at high strain rates beyond $\dot{\epsilon} \sim 280$ shown in figure 1d obtained from the model also exhibits no inherent scale in the magnitudes of the stress drops. The distribution of stress drop magnitudes, $D(\Delta\phi)$, shows a power law $D(\Delta\phi) \sim \Delta\phi^{-\alpha}$. This is shown in figure 3 (o) along with the experimental points (+ along with the arrows) corresponding to $\dot{\epsilon}_a = 8.3 \times 10^{-5} \text{ s}^{-1}$. It is clear from figure 3 that both experimental

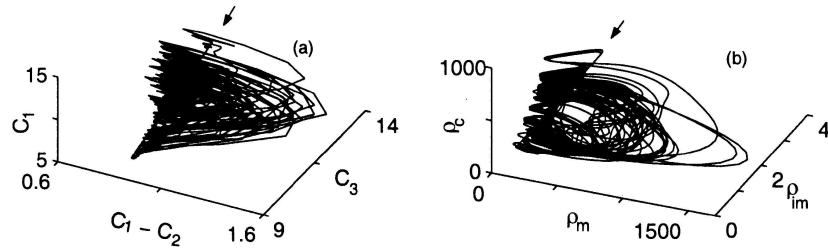


Figure 2. (a) Reconstructed experimental attractor, (b) attractor from the model for $N = 100$, $j = 50$.

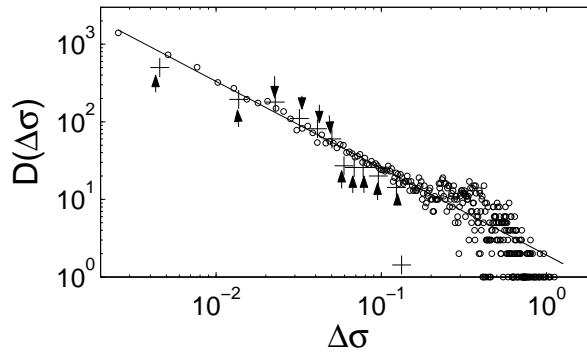


Figure 3. Distributions of the stress drops from the model (\circ) for $N = 1000$, from experiments ($+$ with arrows). Solid line is guide to the eye.

and theoretical points show a scaling behavior with an exponent value $\alpha \approx 1.1$. The distribution of the durations of the drops $D(\Delta t) \sim \Delta t^{-\beta}$ also shows a power law with an exponent value $\beta \approx 1.3$. The conditional average of $\Delta\phi$ denoted by $\langle \Delta\phi \rangle_c$ for a given value of Δt behaves as $\langle \Delta\phi \rangle_c \sim \Delta t^{1/x}$ with $x \approx 0.65$. The exponent values satisfy the scaling relation $\alpha = x(\beta - 1) + 1$ quite well.

3.1 Dynamical characterization of the cross-over

The next natural step is to study the distribution of Lyapunov exponents, λ_i ($i = 1, \dots, M = 3N + 1$) using eqs (1)–(4) for the entire range of strain rates where the interesting dynamics is seen. As the existence of a limiting distribution of Lyapunov exponents [19] as a function of system size [20] is an important issue for spatially extended systems, we have verified this point for various values of strain rate [20]. Note that this also implies the existence of a limiting Lyapunov exponent (LLE) as a function of system size. As the gross changes in the dynamics can be understood by following the largest LLE, we have shown the average LLE in figure 4 as a function of the strain rate for $N = 500$ (left panel). As can be seen, the LLE practically vanishes around $\dot{\epsilon} = 250$. For $\dot{\epsilon} \geq 250$, the value of the LLE is $\sim 5 \times 10^{-4}$. We have also followed the changes in the distribution of Lyapunov exponents as a function of strain rate. We find that in the mid-chaotic region, the distribution of

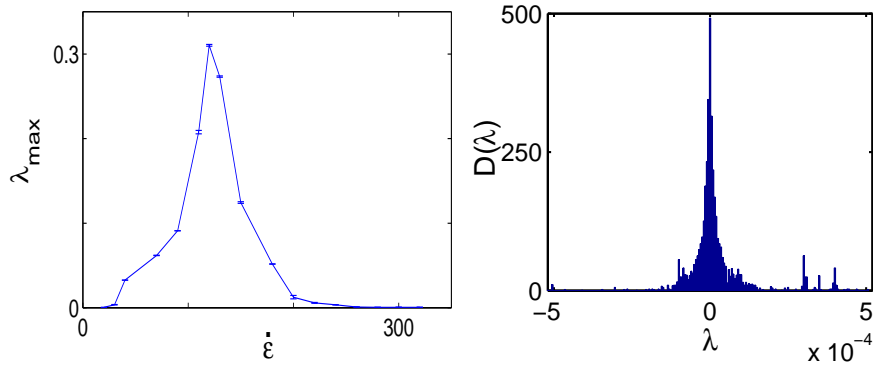


Figure 4. The largest Lyapunov exponent of the model for $N = 500$ (left panel). The peaked nature of the distribution of the null Lyapunov exponents (right panel) at $\dot{\epsilon} = 280$ for $M = 10,000$.

Lyapunov exponents is quite broad (see [20]). However, as we increase the strain rate further into the power-law regime of strain rate (from $\dot{\epsilon} = 250$), the LLE becomes vanishingly small ($\approx 5.2 \times 10^{-4}$). Below a resolution of $\sim 10^{-4}$, exponents close to each other cross as a function of time even as the first few exponents are distinguishable. However, the (time averaged) distribution remains unaffected. In this regime, the number of null exponents (almost vanishing) increases gradually reaching a value $\approx 0.38M$ in the range $[-0.00052, 0.00052]$ at $\dot{\epsilon} = 280$. The finite density of null exponents has a peaked nature (figure 4 (right panel)) in the interval $250 \leq \dot{\epsilon} \leq 700$, a result similar to GOY shell model for turbulence [21]. Thus, the spectrum changes from a set of both positive and negative, but few null exponents in the chaotic region, to a *dense set of null exponents and negative exponents with no positive exponents* in the scaling regime, as if most exponents are pushed toward the zero value. As null exponents correspond to a marginal situation, their finite density in the power-law state implies that most spatial elements are perpetually close to the marginal state.

3.2 Visualization of dislocation configurations

The marginal nature of the dislocation configurations in the power-law regime can be visualized by studying the slow manifold of the model [16,22]. This method also allows us to track the configurations during cross-over. The geometry of the slow manifold has been recently analysed [16]. Here we recall some relevant results on the slow manifold of the original model ($D = 0$) and use them when the spatial coupling is switched on. Slow manifold expresses the fast variable in terms of the slow variables, conventionally done by setting the derivative of the fast variable to zero [16]. Thus, setting $\dot{\rho}_m = 0$ gives ρ_m as a function both the slow variables, i.e., $\rho_m = \rho_m(\rho_{im}, \phi)$. Instead, we use ρ_m in terms of a single slow variable $\delta = \phi^m - \rho_{im} - a$. Using $\dot{\rho}_m = g(\rho_m, \phi) = -b_0 \rho_m^2 + \rho_m \delta + \rho_{im} = 0$, and noting that $\rho_m > 0$, we get two solutions $\rho_m = [\delta + (\delta^2 + 4b_0 \rho_{im})^{1/2}] / 2b_0$, one for $\delta < 0$ and

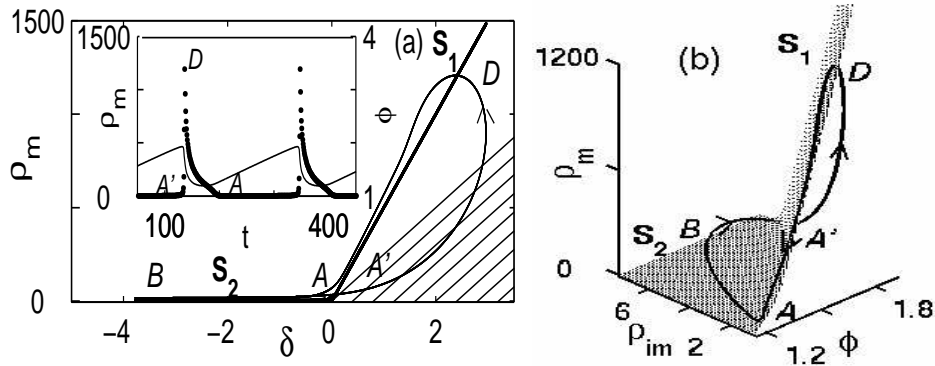


Figure 5. (a) Bent slow manifold S_1 and S_2 (thick lines) with a simple trajectory for $\dot{\epsilon} = 200$ and $m = 3$. Inset: ρ_m (dotted curve) and ϕ . (b) Same trajectory in the $(\phi, \rho_{im}, \rho_m)$ space.

another for $\delta > 0$. We note that δ takes small positive and negative values as both ρ_{im} and ϕ are small and positive. For regions of $\delta < 0$, as b_0 is small ($\sim 10^{-4}$), we get $\rho_m/\rho_{im} \approx -1/\delta$ which takes small values defining a part of the slow manifold, S_2 . Since physically pinned configuration of dislocations implies small mobile density and large immobile density, we refer to the region of S_2 as the ‘pinned state of dislocations’. Further, larger negative values of δ correspond to strongly pinned configurations, as they refer to smaller ratio of ρ_m/ρ_{im} . Corresponding to $\delta > 0$, another connected piece S_1 is defined by large values of ρ_m , given by $\rho_m \approx \delta/b_0$, which we refer to as the ‘unpinned state of dislocations’. S_2 and S_1 are separated by $\delta = 0$, which we refer to as the *fold line* [16] (see below). A plot of the slow manifold in the δ - ρ_m plane is shown in figure 5a along with a simple monoperoiodic trajectory describing the changes in the densities during one loading–unloading cycle. The inset shows $\rho_m(t)$ and $\phi(t)$. For completeness, the corresponding plot of the slow manifold in the $(\rho_m, \rho_{im}, \phi)$ space is shown in figure 5b, along with the trajectory and the symbols. Note that in this space, S_2 and S_1 are separated by a fold given by $\delta = \phi^m - \rho_{im} - a = 0$, and hence the name *fold line*. The correspondence between figure 5a and figure 5b is also clear. Note that the burst in ρ_m (inset in figure 5a) corresponds to the segment $A'DA$ in figures 5a and 5b.

We first note that the yield drop is a consequence of the generation of mobile dislocations. Thus, even though stress is an average over the entire sample, some information is contained in it. As we shall see, considerable insight can be had by visualizing the dislocation configurations just before the yield drop and after. We shall do this both in the chaotic regime as well as in the region of the power-law distribution of the stress drops. Since the yield drop occurs when $\bar{\rho}_m(t)$ grows rapidly, it is adequate to examine the spatial configurations on the slow manifold at the onset and at the end of typical yield drops. Figures 6a, 6b and 6c, 6d show respectively, plots of $j, \delta(j), \rho_m(j)$ for the chaotic state $\dot{\epsilon} = 120$ and the power-law state $\dot{\epsilon} = 280$, at the onset and at the end of an yield drop. It is clear that for $\dot{\epsilon} = 120$, both at the onset and at the end of a typical large yield drop

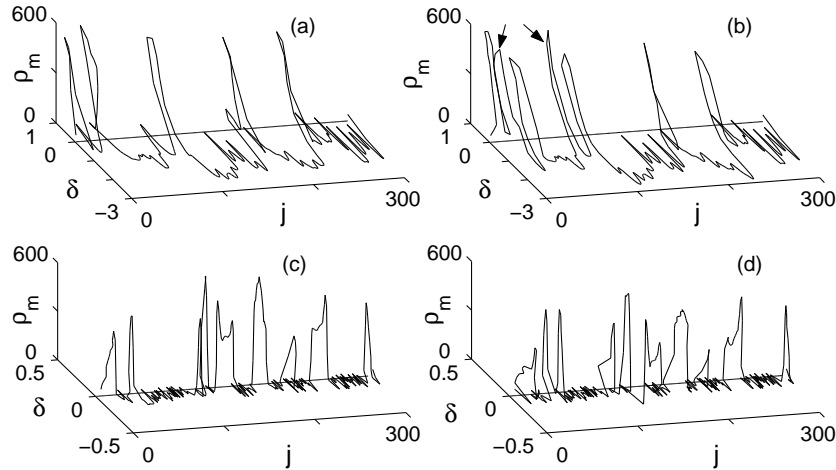


Figure 6. Dislocation configurations on the slow manifold at the inset and at the end of an yield drop: (a) and (b) for $\dot{\epsilon} = 120$ (chaos), and (c) and (d) for $\dot{\epsilon} = 280$ (scaling).

(figures 6a, 6b), most $\rho_m(j)$ s are small with large negative values of $\delta(j)$, i.e., most dislocations are in a *strongly pinned state*. The arrows show the increase in $\rho_m(j)$ at the end of the yield drop. In contrast, in the scaling regime, for $\dot{\epsilon} = 280$, most dislocations are at the threshold of unpinning with $\delta(j) \approx 0$, both at the onset and at the end of the yield drop (figures 6c, 6d). This also implies that they remain close to this threshold all the time (figure 6d). Since $\delta(j) \approx 0$ (for most j s) refers to a marginally stable state, it can produce almost any response. This in turn implies that the magnitudes of yield drops $\Delta\phi$ are scale-free. We have verified that the edge-of-unpinning picture is valid in the entire scaling regime for a range of $N = 100$ – 1000 . Further, the number of spatial elements reaching the threshold of unpinning $\delta = 0$, during an yield drop increases as we approach the scaling regime.

4. Summary and discussion

We summarize the salient features of the cross-over and comment on them wherever necessary.

- (a) The cross-over is smooth as changes in the Lyapunov spectrum are gradual.
- (b) The power law here is of purely dynamical origin. This situation is to be contrasted with coupled map lattices where the power law arises with the inclusion of threshold on each element describing the local dynamics [23]. In our case, the pinning and unpinning of dislocations is fully dynamical and is completely determined by the global feed defined by eq. (4). We note that the stress developed depends on the plastic strain rate (eq. (4)), which, however, decides the rate of production of the mobile density (fifth and sixth terms in eq. (1)). Indeed, the set of equations also controls internal relaxation

mechanism through a competition of the time-scales due to the applied strain rate and other time-scales determined by various dislocation mechanisms. It is this competition that leads the reverse Hopf bifurcation at high strain rates which in turn limits the average stress drop amplitude to small values [16] in its neighborhood. Note that this implies that the applied strain rate nearly balances the plastic strain rate. In other words, *the system is close to a critical state*. This can only lead to partial relaxation of the plastic strain.

- (c) The power-law regime of stress drops occurring at high strain rates belongs to a different universality class compared to SOC type systems as it is characterized by a dense set of null exponents. As zero exponents correspond to a marginal situation, their finite density physically implies that most spatial elements are close to criticality. This is supported by the *geometrical picture of the slow manifold* where most dislocations are at the threshold of unpinning, $\delta = 0$. This must be contrasted with the non-uniqueness of the nature of the Lyapunov spectrum in the few models studied so far. For instance, no zero and positive exponents, zero exponent in the large N limit etc., have been reported [24]. (Often, the nature of Lyapunov spectrum is inferred based on other dynamical invariants [24].) More significantly, the dense set of null Lyapunov exponents themselves follow a power law. Further, we note that the Lyapunov spectrum evolves from a set of both positive and negative, but few null exponents in the chaotic region, to a dense set of marginal exponents as we reach the power-law regime.
- (d) The dense set of null exponents found in our model is actually similar to that obtained in shell models of turbulence where the power law is seen at high drive values [21]. However, there are significant differences. First, we note that the shell model [21] cannot explain the cross-over as it is only designed to explain the power-law regime. Further, the maximum Lyapunov exponent is large for small viscosity parameter ($\lambda_1 \propto \text{viscosity}^{-1/2}$) in shell models [21] in contrast to near-zero value in our model. Finally, we state here that a detailed comparison between our model and the GOY model has been studied in detail [20].

In summary, the original model extended to include the spatial degrees of freedom explains the cross-over in the dynamics from chaotic to power-law regime as observed in experiments. For the sake of completeness, we mention here that the model also exhibits the uncorrelated bands, the hopping type and the continuously propagating type as the strain rate is increased as seen in experiments [25]. Thus, the dynamical model captures the full dynamics of the PLC effect. From a dynamical point of view, the changes in the Lyapunov spectrum provides a good insight into the underlying mechanism controlling the cross-over. The slow manifold analysis, applied to study the cross-over, is particularly useful in giving a geometrical picture of the spatial configurations in the chaotic and scaling regimes. Further, this is also the first time a methodology has been introduced wherein dislocation configurations can be realized. Further, this picture explains the origin of small amplitude stress drops at high strain rates. Finally, this is the first fully dynamical model for the PLC effect explaining almost all features of the PLC effect in addition to explaining the cross-over from chaotic to power-law regime. The latter aspect should be of interest to the area of dynamical systems.

Acknowledgements

The work reported here is a fruitful completion of the study of the PLC effect using the model introduced almost twenty five years ago in collaboration with the author's colleagues at Kalpakkam, D Sahoo and M C Valsakumar. The author is grateful for their collaboration. The author also wishes to acknowledge the contributions of his several former students, M Bekele, S J Noronha, S Rajesh and M S Bharathi. This work is supported by Department of Science and Technology, New Delhi, India.

References

- [1] A J Lichtenberg and M A Liberman, *Regular and chaotic motion* (Springer-Verlag, New York, 1992)
- [2] P Bak, C Tang and K Wiesenfeld, *Phys. Rev. Lett.* **59**, 381 (1987); *Phys. Rev.* **A38**, 364 (1988)
- [3] H J Jensen, *Self-organized criticality* (Cambridge University Press, Cambridge, 1998)
- [4] G Ananthkrishna, S J Noronha, C Fressengeas and L P Kubin, *Phys. Rev.* **E60**, 5455 (1999)
- [5] M S Bharathi, M Lebyodkin, G Ananthkrishna, C Fressengeas and L P Kubin, *Phys. Rev. Lett.* **87**, 165508 (2001)
- [6] G Ananthkrishna and M C Valsakumar, *J. Phys.* **D15**, L171 (1982)
- [7] L P Kubin, C Fressengeas and G Ananthkrishna, in *Collective Behavior of Dislocations* edited by F R N Nabarro and M S Deuserby (North-Holland, Amsterdam, 2002) vol. 11, p. 101
- [8] A H Cottrell, *Dislocations and plastic flow in crystals* (Clarendon Press, Oxford, 1953)
- [9] M A Lebyodkin, Y Brechet, Y Estrin and L P Kubin, *Phys. Rev. Lett.* **74**, 4758 (1995)
- [10] G Ananthkrishna and M C Valsakumar, *Phys. Lett.* **A95**, 69 (1983)
- [11] G Ananthkrishna *et al*, *Scrip. Mater.* **32**, 1731 (1995)
- [12] S J Noronha, G Ananthkrishna, L Quouuire, C Fressengeas and L P Kubin, *Int. J. Bifurcat. Chaos* **7**, 2577 (1997)
- [13] See, for instance, F Heslot, B Castaing and A Libchaber, *Phys. Rev.* **A36**, 5780 (1987)
- [14] M S Bharathi and G Ananthkrishna, *Europhys. Lett.* **60**, 234 (2003)
- [15] M S Bharathi and G Ananthkrishna, *Phys. Rev.* **E67**, 065104R (2003)
- [16] S Rajesh and G Ananthkrishna, *Physica* **D140**, 193 (2000)
- [17] M Ding, C Grebogi, E Ott, T Sauer and J A Yorke, *Phys. Rev. Lett.* **70**, 3872 (1993)
- [18] D Broomhead and G King, *Physica* **D20**, 217 (1987)
- [19] T Bohr, M H Jesen, G Paladin and A Vulpiani, *Dynamical systems approach to turbulence* (Cambridge University Press, Cambridge, 1992)
- [20] G Ananthkrishna and M S Bharathi, *Phys. Rev.* **E70**, 02611 (2004)
- [21] M Yamada and K Ohkitani, *Phys. Rev. Lett.* **60**, 983 (1988)
- [22] A Milik, P Szmolyan, H Loffelmsnn and E Grobller, *Int. J. Bifurcat. Chaos* **8**, 505 (1998)
- [23] S Sinha and D Biswas, *Phys. Rev. Lett.* **77**, 2010 (1993)
S Sinha, *Phys. Rev.* **E49**, 4832 (1994); *Phys. Lett.* **A199**, 365 (1995)
- [24] A Erzan and S Sinha, *Phys. Rev. Lett.* **66**, 2750 (1991)
M de Sousa Vieira and A J Lichtenberg, *Phys. Rev.* **E53**, 1441 (1996)
B Cessac, Ph Blanchard and T Kruger, *Phys. Rev.* **E64**, 016133 (2001)
- [25] M S Bharathi, S Rajesh and G Ananthkrishna, *Scr. Mater.* **48**, 1355 (2003)